Lightweight Wearable Fingertip Haptic Device with 3-DOF Directional Force Feedback based on Fingernail Stimulation

Yunxiu Xu[1,2], Siyu Wang[1], and Shoichi Hasegawa[1], *Member, IEEE*

***Abstract*—Wearable haptic devices face a trade-off between providing rich feedback and preserving natural fingertip sensation. Current multi-DOF systems encumber the fingerpad, interfering with fingerpad sensory capabilities, while lightweight devices offer limited 1-DOF feedback. To address this, we present a 5.24 g, three-degree-of-freedom (3-DOF) haptic device that stimulates mechanoreceptors around the fingernail, leaving the fingerpad unobstructed. It uses two string-pulling motors for distal-proximal feedback and an arc-shaped pin motor for radial-ulnar stimulation to generate directional force vectors. This approach is grounded in the physiology of directionally-sensitive slowly adapting type 2 (SA2) mechanoreceptors. Experimental results demonstrate that the proposed 3-DOF approach improves weight and friction discrimination over single-DOF pressure feedback. Moreover, it delivers directional cues during static contact, a capability absent in vibrotactile systems, and achieves higher overall user satisfaction. By preserving fingertip sensation, the proposed device enables simultaneous interaction with virtual and physical objects, making it suitable for mixed reality applications.**

***Index Terms*—Fingertip tactile interface, haptic feedback, nail wall stimulation, tactile discrimination, wearable haptic device.**

I. Introduction

THE pursuit of immersive virtual reality (VR) experiences has driven rapid advancements in fingertip haptic feedback. These technologies enable dexterous manipulation in virtual environments. However, a primary challenge in wearable haptics is the trade-off between delivering rich, multi-dimensional feedback and preserving natural hand dexterity. Many existing systems either offer limited feedback or encumber the fingerpad, preventing precision grips and interfering with the ability to interact with real objects. This limitation arises from the conventional approach where the device's end-effector is placed on the fingerpad, transmitting forces from actuators typically mounted on the back of the finger.

The fingertip contains four types of mechanoreceptive units (Meissner corpuscles, Pacinian corpuscles, Merkel's disks, and Ruffini endings) with distinct spatial and temporal response characteristics [1], [2]. Birznieks et al. [3] demonstrated that slowly adapting type 2 (SA2) mechanoreceptors around the fingernail borders reliably respond to forces applied to the fingerpad. These mechanoreceptors show directional preferences across all angles. This physiological finding provides the scientific foundation for the proposed approach. Nail wall stimulation can convey force information without interfering with natural fingerpad mechanoreceptors.

Tangential force feedback offers richer information content compared to normal force alone. Tamura and Okamoto [4] established that the tangential component of contact force contains more detailed textural information than the normal component. Directional force vectors, rather than simple pressure magnitude, are necessary for distinguishing physical properties. During object manipulation, weight is perceived through the direction of gravitational force, while friction is identified by the characteristic tangential resistance that occurs during sliding.

Achieving 3-DOF feedback without occupying the fingertip presents technical challenges, particularly for distal-proximal directional stimulation. Radial-ulnar feedback, referring to finger lateral directions as illustrated in Fig. 1, can be delivered through lateral nail wall stimulation using simple actuator configurations. In contrast, distal-proximal directions require activation of mechanoreceptors near the proximal phalanx region. Conventional motor-based structures face severe space and mounting constraints in this area.

To address these challenges, we introduce a lightweight (5.24 g), 3-DOF nail wall-based haptic device that preserves fingerpad sensation for mixed reality interactions. The design features an actuation mechanism grounded in the physiology of directionally-sensitive SA2 mechanoreceptors around the fingernail borders. We provide an experimental validation demonstrating that the proposed approach improves weight and friction discrimination over single-DOF systems and enables static force rendering.

II. Related Work

The development of wearable fingertip haptic devices has focused on balancing feedback richness with preserving natural interaction capabilities. A critical design consideration is whether the device occludes the fingerpad, as this directly impacts the user's ability to interact with real-world objects, which is necessary for mixed reality applications. We review

[1]Y. Xu, S. Wang, and S. Hasegawa are with the Department of Information and Communication Engineering, Institute of Science Tokyo, Yokohama, Japan (e-mail: yunxiu@haselab.net).

[2]Y. Xu is also with The University of Tokyo, Tokyo, Japan.

Corresponding author: Yunxiu Xu (e-mail: yunxiu@haselab.net).

This work was supported by JST, the establishment of university fellowships towards the creation of science and technology innovation, Grant Number JPMJSP2180, and JSPS KAKENHI Grant Number 23H03432 and 25KJ1279.

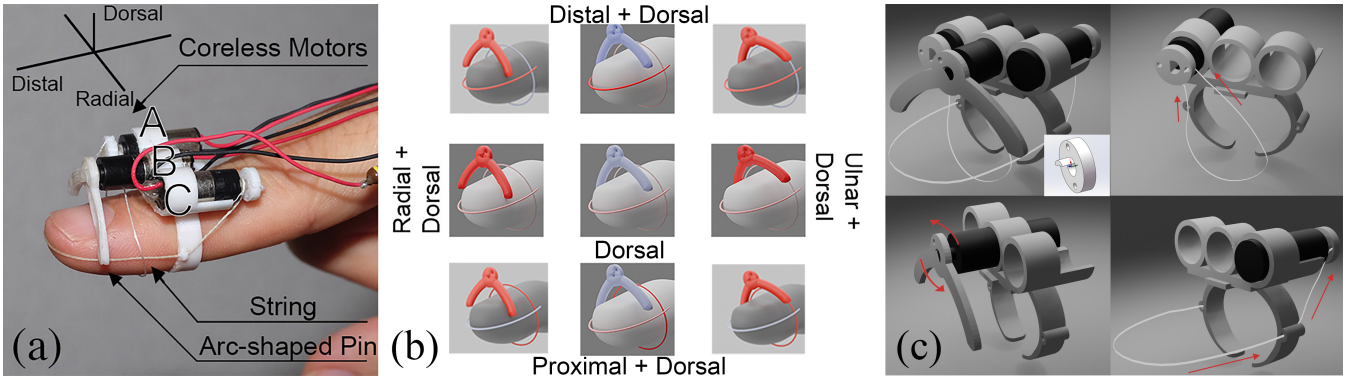

Fig. 1. Proposed 3-DOF nail wall-based haptic feedback device. (a) Device worn on a finger (Motors A–C, two strings, arc-shaped pin; 5.24 g). (b) Nine directional patterns (3×3 grid); red indicates active actuators. (c) Mechanical principle of 3-DOF actuation showing each motor's individual action. The top-left panel shows the full assembly; an inset at bottom-right shows the coupler and D-shaped shaft connecting the motor to the string spool. Motor A (top-right) pulls a string to generate distal force. Motor B (bottom-left) rotates bidirectionally to produce radial and ulnar forces. Motor C (bottom-right) pulls a string to generate proximal force.

mechanical design strategies for maintaining fingerpad accessibility.

A. Wearable Devices and Fingertip Obstruction

1) Vibration Feedback (Open Fingertip): Vibrotactile feedback remains a common approach for unobstructed fingertip haptics due to its compact form factor. The concept of nail-mounted tactile devices was pioneered by Ando et al. [5], who introduced a fingernail-mounted tactile display for augmented reality that left the fingerpad free. Recently, Messerschmidt et al. [6] advanced this concept with PhantomFolds, a nail-mounted device enabling spatial vibrotactile feedback. While these open-fingerpad designs preserve cutaneous sensitivity, vibrotactile feedback has fundamental limitations: it requires continuous sliding motion to generate sensation and cannot inherently convey static directional forces, which are necessary for weight and grasp perception.

2) Single-DOF Pressure Feedback (Open Fingertip): Several devices focus on Single-DOF normal force. Aoki et al. proposed a lightweight device using thin wires to apply normal force via cutaneous sensing [7]. Han et al. [8] presented HydroRing, which uses liquid flow to deliver pressure. These designs enable mixed-reality haptic interactions without impeding natural tactile sensation. However, they are limited to force magnitude. Weight and friction perception depend on directional force vectors (shear forces), which cannot be distinguished by 1-DOF pressure alone.

3) Multi-DOF Devices (Typically Occluded): To render complex interactions, Multi-DOF devices typically apply forces directly to the fingertip. Prattichizzo et al. [9] presented a 3-DOF wearable device using a parallel robot structure. Chinello et al. [10] developed a 3RRS wearable device, and Tsetserukou et al. [11] introduced LinkTouch. Yem et al.'s FinGAR [12] represents another multi-modal approach combining mechanical and electrical stimulation. While these systems provide rich directional cues, they generally rely on end-effectors that cover the fingerpad, impairing dexterous manipulation and preventing direct contact with real objects. Recent efforts have attempted to mitigate this bulk. Kim et al. [13] introduced StringTouch, a lightweight tendon-driven interface. However, even such optimized designs often require rigid side guides that can obstruct finger adduction or natural inter-finger contact. The challenge remains to provide 3-DOF directional feedback without occluding the fingerpad or hindering hand dexterity.

B. Emerging Approaches for Unobstructed Haptics

1) Haptic Redirection: Recent trends explore redirecting haptic sensations to leave the active fingerpad free. Nakayama et al. [14] demonstrated that feedback to the fingernail sides creates referred sensations. However, this research focuses on electrical stimulation, which differs from the perception of mechanical stimulation. Palmer et al.'s [15] wrist-worn device and Moriyama et al.'s forearm device [16] relocate forces entirely. While effective for unencumbered interaction, these methods often rely on sensory illusions or remote stimulation, which may lack the directness and fidelity of fingertip-applied forces.

2) Non-Contact and Novel Haptic Feedback: Non-contact technologies, such as ultrasound (Matsubayashi et al. [17], [18], Carter et al. [19], Iwamoto et al. [20]) and airflow (Gupta et al. [21]), avoid mechanical interference. Singh et al. [22] developed a ferro-fluid based portable display to provide tactile cues. However, these approaches typically require line-of-sight, have high power consumption, and offer limited force magnitude compared to wearable mechanical devices.

C. Physiological and Perceptual Basis

The proposed approach addresses the trade-off between feedback richness and fingerpad occlusion by exploiting SA2 mechanoreceptors around the fingernail borders. As detailed by Longo et al. [23] and Birznieks et al. [3], these receptors respond to forces applied to the fingerpad with directional preferences. Unlike the fingerpad, the nail border is dominated by SA2 receptors sensitive to skin stretch [24]. This anatomical specialization enables the proposed design: the nail wall is stimulated to convey 3-DOF directional forces, leaving the fingerpad free for mixed reality interaction.

III. System Overview

A. Hardware Design

We employed a ring structure to mount three motors on the side of the fingernail. To ensure a secure fit across different finger sizes, the inner ring was lined with Sorbothane, a viscoelastic damping material (Sorbothane, Inc., Kent, OH, USA), with its thickness adjusted for each participant to minimize slippage (inset in Fig. 4(a)). Distal-proximal feedback is provided by a tendon-driven system actuated by Motors A and C, as illustrated in Fig. 1(c). Each motor pulls a thin string (0.26 mm diameter, ultra-high-molecular-weight polyethylene) wound on a spool. The spool is mounted on a coupler that connects to the motor's D-shaped output shaft, forming a 1 mm diameter shaft assembly (inset in Fig. 1(c)). The routing paths for the two strings are distinct to create differentiated directional cues. For Motor A (distal force), the string is routed directly from the spool around the distal phalanx. For Motor C (proximal force), the string first passes through an integrated guide on the main housing before wrapping around the phalanx. Both strings terminate at guide loops on the opposite side of the ring. This routing strategy, which avoids complex pulleys, allows the motors to apply tension at slightly different angles to generate distinct distal and proximal sensations. Motor B, equipped with an arc-shaped pin, directly stimulates the radial and ulnar sides of the fingernail for lateral feedback. Dorsal pressure sensation is achieved through balanced activation of both string motors. In addition to directional force rendering, Motor A is also used to provide vibrotactile feedback by rapidly modulating the string tension. The key performance parameters for this modality are reported in Section III-B, and the rendering method is detailed in Section III-E.

For actuation, we selected 6-mm planetary DC gear motors (Zhaowei, Shenzhen, China). Each motor has a diameter of 6 mm and a length of 12 mm. The arc-shaped pin motor (shown in Fig. 1 (a)) operated with a gear ratio of 27.41:1, while the string-pulling motors functioned with a gear ratio of 5.14:1. These gear ratios were selected to balance adequate force output with back-drivability, ensuring natural finger manipulation.

The hardware setup consisted of a microcontroller, motor driver, and actuators. For the microcontroller, we selected the PIC32MK0512MCJ064-I/PT (USA, Microchip Technology), which received serial port signals from the personal computer (PC) containing haptic data. This controller was capable of outputting up to 9 channels of pulse width modulation (PWM) signals, which met the requirements for controlling multiple motors. We used the DRV8434e (USA, Texas Instruments) driver with a current controller to regulate the output current for each motor. This driver enabled constant force output control based on current feedback. This control architecture built upon established string-based haptic feedback approaches [25], [13], extending the design to support multi-dimensional force feedback.

Prior to use, the device required individual calibration for each user to accommodate personal differences in tactile sensitivity and perception thresholds. This process determines individual thresholds and normalizes perceptual intensity. Detailed procedures are described in Sections III-C and III-D.

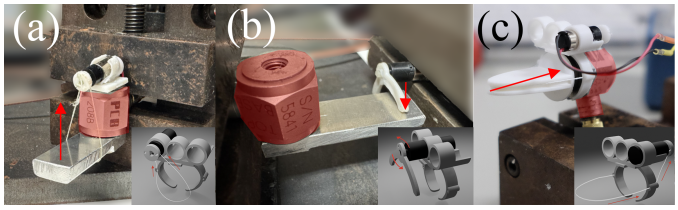

Fig. 2. Experimental setup for force measurement. The red semi-transparent overlay indicates the PCB 208B force sensor, with its central axis aligned to the direction of the applied force. (a) Measurement of string tension from Motor A. (b) Measurement of lateral force from Motor B's arc-shaped pin. (c) Measurement of string tension from Motor C. Insets illustrate the corresponding mechanical actuation mechanism for each motor.

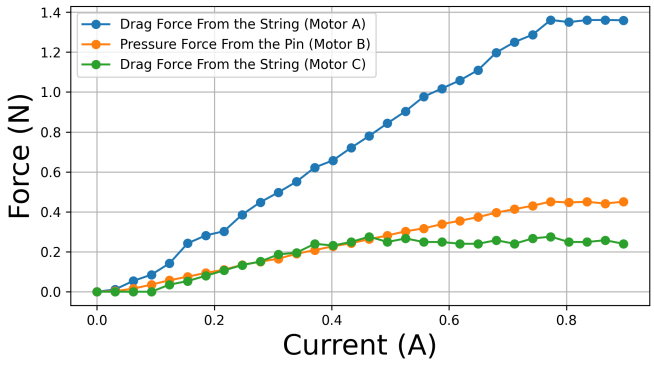

Fig. 3. Force output characteristics of the three motors as a function of target current. The graph shows the drag force from the strings (Motor A and Motor C) and the pressure force from the arc-shaped pin (Motor B). All motors exhibit a linear relationship between current and output force.

B. Hardware Performance

We measured the force output of the system using a PCB 208B force sensor (PCB Piezotronics, USA). The measurement setup, shown in Fig. 2, was designed to replicate the device's interaction with the finger as closely as possible, addressing potential force losses from friction. The sensor was positioned such that its central axis aligned with the force vector of each actuator: string tension for Motors A and C, and lateral push for Motor B. This arrangement ensured that the measured forces are a reasonable proxy for the forces delivered to the user's finger. While multiple repeated measurements for a statistical analysis were not performed, the force output exhibited a predictable and linear relationship with the input current for all motors, as shown in Fig. 3. This linearity indicates consistency and repeatability in the actuator's performance. The results showed that Motor A generated a maximum static force of 1.38 N and could produce 90 Hz vibrations with a maximum peak-to-peak amplitude of 0.21 N, Motor B (arc-shaped pin) produced 0.42 N, and Motor C achieved 0.29 N. Furthermore, any static friction losses are implicitly compensated for during the user-specific perceptual calibration procedure, which maps motor commands to perceived sensation rather than theoretical force output.

C. Single-Channel Threshold Calibration

1) Procedure for Each Channel: We conducted individual threshold calibration for each of the three motors: Motor A, Motor B, and Motor C, as shown in Fig. 4(a) and (b). For this calibration procedure, participants wore the haptic device while the calibration software was running. The interface provided text-based instructions to guide them through the process. Participants controlled the motor force intensity using the "+" and "-" keys on the keyboard and could see the current output intensity value on the screen in real-time. For each motor, participants started with a low current output. They incrementally increased the intensity by pressing the "+" key until they reported the first perception of the stimulus. This value was recorded as the lower threshold (L_i) for that motor. Participants then continued increasing the intensity until they reached a level they described as "approaching but not exceeding comfort" or until the motor reached the maximum current. This value was recorded as the upper threshold (U_i).

2) Threshold Recording: For each participant, we recorded the lower (L_i) and upper (U_i) thresholds for all three motors ($i \in \{A, B, C\}$), where A, B, and C represent the individual motor units. These thresholds were used to establish the operational range for each motor. The upper threshold determined during this calibration was mapped to 100% motor output intensity in subsequent experiments. This calibration was performed once for each participant before the main experiments began. The device was not removed until all tasks were completed, and its secure fit, ensured by the Sorbothane lining, maintained the validity of this single calibration throughout the session.

D. 3-DOF Perceptual Normalization

1) Reference Channel Selection: For perceptual consistency across different feedback directions, we selected the "Distal" (Motor A) channel as the reference. This channel has been used in previous studies and applies pressure to the fingerpad from a typical and stable mounting position, making it an ideal reference point.

2) Intensity Matching Between Motors: To achieve perceptually equivalent stimulus intensities across different motors, we employed a direct comparison method. We defined the midpoint of the reference motor, $M_A = (L_A + U_A)/2$, as the comparison standard. For each of the other two motors, we performed intensity matching through the following procedure:

1) Each motor was initially set to output at its own midpoint, $M_i = (L_i + U_i)/2$.
2) Participants alternately experienced the reference motor (Motor A) and the test motor. Each stimulus lasted 3 seconds and was separated by a 2-second pause with no output.
3) Participants directly compared the perceived intensities and adjusted the gain (g_i) of the test motor using the "+" or "-" buttons until both motors produced perceptually equivalent sensations.
4) The final gain value (g_i) was recorded for each motor, with the reference motor having a gain of $g_A = 1.0$.

All subsequent force outputs were mapped according to $F_i^{out} = g_i \cdot F_i^{raw}$. This ensures that equivalent motor commands produce perceptually matched stimulus intensities across all three motors. The gain adjustment step size was set to 0.05, and the actual output value was calculated as $o_i = \mathrm{int}(g_i \cdot M_i)$.

The calibration results for each participant were saved. These results included timestamps, threshold values for all three channels (Distal A, Proximal C, and Radial/Ulnar B), and the corresponding gain values. The reference channel (Distal A) maintained a fixed gain of 1.0, while the other channels' gains were determined through the perceptual matching procedure.

E. Haptic Rendering and Control

For all haptic feedback approaches, the normalized force intensities are mapped to individual motor output ranges using personal calibration parameters. We utilized linear interpolation for direct scaling. This linear mapping aligns with the proportional force-displacement relationship used in virtual coupling (Section IV-A), maintaining consistency with the physics-based rendering approach. While non-linear mappings (e.g., logarithmic) merit future investigation, as human sensory perception often follows Weber's law, this approach preserved relative force differences for the discrimination tasks:

$$u_i = g_i \cdot (I \cdot (U_i - L_i) + L_i) \tag{1}$$

where I represents the normalized intensity (0–1) from force processing, L_i and U_i are the individual lower and upper thresholds from personal calibration (Section III-C), and g_i is the perceptual gain adjustment factor (Section III-D). This process ensures that equivalent normalized intensities produce perceptually matched stimuli across participants and feedback modalities.

The system implemented three distinct haptic rendering approaches:

Vibrotactile Feedback: This condition served as a comparison baseline representing conventional vibrotactile haptic devices. This approach implemented physics-based vibrotactile rendering that mapped contact force variations to vibration intensity. This method is grounded in research showing that the rate of tangential force variation correlates with tactile perception [26]. It is also supported by findings that vibrotactile stimulation can represent friction without actual tangential forces [27]. When sliding across surfaces with varying friction properties, users perceived differences in resistance through force-modulated vibration.

$$F_l = \sqrt{F_x^2 + F_y^2} \tag{2}$$

where F_x and F_y represent the local force components along the radial-ulnar and distal-proximal axes, respectively. The lateral force magnitude F_l directly correlated with surface friction. Higher friction surfaces generated larger tangential forces during sliding contact, which were then converted into proportionally stronger vibrotactile stimuli.

For vibration scaling, force normalization boundaries were established:

$$F_{l,min} = \sqrt{F_{th,x}^2 + F_{th,y}^2} \tag{3}$$

$$F_{l,max} = \sqrt{F_{max,x}^2 + F_{max,y}^2} \tag{4}$$

where $F_{th,x}$, $F_{th,y}$ represented minimum detectable forces, and $F_{max,x}$, $F_{max,y}$ represented maximum expected forces along each axis. These normalization boundaries were determined through preliminary experiments with two experienced users; the upper bounds ($F_{max,i}$) were set to the 90th percentile of recorded force distributions, and the lower thresholds ($F_{th,i}$) were set to 0.01 N to filter measurement noise.

The normalized vibration intensity was calculated as:

$$A_v = \begin{cases} 0, & F_l \le F_{l,min} \\ \dfrac{F_l - F_{l,min}}{F_{l,max} - F_{l,min}}, & F_l > F_{l,min} \end{cases} \tag{5}$$

The vibrotactile stimulus was generated as a 90 Hz sinusoidal wave with peak-to-peak voltage amplitude corresponding to A_v, activated only when relative velocity between the finger and object surfaces was detected:

$$V_{m,A}(t) = \begin{cases} A_v \cdot [\sin(2\pi f_v t) + 1] & \text{if } |\mathbf{v}_r| > 0 \\ 0 & \text{otherwise} \end{cases}. \tag{6}$$

where $f_v = 90$ Hz was selected to stimulate Pacinian corpuscles, the mechanoreceptors most sensitive to vibrotactile stimuli and responsible for texture perception, and $\mathbf{v}_r$ represents the relative velocity between finger and object surfaces. This frequency choice is supported by empirical evidence showing natural finger sliding produces vibrations around 89 Hz [28]. The sinusoidal signal was DC-offset to ensure all signal values remained above zero, thereby preventing the motor from reversing its output direction. This approach focused on steady-state sliding friction rather than stick-slip transitions. While stick-slip phenomena are indeed valid friction cues, the objective of this study was to isolate and evaluate directional tangential force feedback as the primary information channel. Including stick-slip dynamics would introduce additional perceptual cues beyond the spatial directional forces that constitute the core contribution of the proposed 3-DOF nail wall stimulation approach. To ensure that experimental results reflected the performance of directional force feedback specifically, rather than the combined effect of multiple friction-related phenomena, we focused on smooth sliding interactions where directional tangential forces served as the primary discriminative feature.

Single-Degree-of-Freedom Pressure Feedback: This condition served as a baseline comparison representing conventional single-actuator haptic devices. Rather than displaying only normal force, this approach integrated all three force components into a single pressure magnitude, delivered through one actuator. This design choice reflected that tangential forces often exceed normal forces during object manipulation tasks, potentially masking the subtler gravitational cues of weight. The 1-DOF condition provided all available force information but without directional distinction. This served as a control condition to evaluate the benefits of multi-dimensional feedback. This approach captured both tangential interactions and normal contact pressure using the total force magnitude $F_{tot} = \sqrt{F_x^2 + F_y^2 + F_z^2}$, where F_z represented the dorsal-ventral force component normal to the fingerpad.

The pressure normalization bounds incorporated all three axes:

$$F_{p,min} = \sqrt{\sum_{j \in \{x,y,z\}} F_{th,j}^2}. \tag{7}$$

$$F_{p,max} = \sqrt{F_{max,x}^2 + F_{max,y}^2 + F_{max,z}^2} \tag{8}$$

$$I_{\text{raw}} = \frac{F_{tot} - F_{p,min}}{F_{p,max} - F_{p,min}}, \tag{9}$$

$$I_p = \max\big(0,\, \min(1,\, I_{\text{raw}})\big). \tag{10}$$

The motor output directly corresponded to the normalized pressure intensity I_p.

3-DOF Directional Feedback: The 3-DOF system provided independent directional force information through multiple actuators using a directional interpolation approach. The two string-pulling motors (Motors A and C) established two fundamental directional vectors, while Motor B provided lateral feedback. Any perceived direction was achieved through weighted combinations of these base vectors.

For normalized force components along each axis $j \in \{x, y, z\}$:

$$\hat{F}_j = \frac{|F_j| - F_{th,j}}{F_{max,j} - F_{th,j}} \tag{11}$$

The directional interpolation weights for the two string motors were calculated as:

$$w_A = \begin{cases} \hat{F}_y & \text{if } F_y > F_{th,y} \text{ (distal direction)} \\ 0 & \text{otherwise} \end{cases} \tag{12}$$

$$w_C = \begin{cases} \hat{F}_y & \text{if } F_y < -F_{th,y} \text{ (proximal direction)} \\ 0 & \text{otherwise} \end{cases} \tag{13}$$

For dorsal (z-axis) forces, both motors contributed equally to create a balanced pressure sensation:

$$w_{dorsal} = \begin{cases} \hat{F}_z & \text{if } F_z > F_{th,z} \\ 0 & \text{otherwise} \end{cases} \tag{14}$$

The final motor outputs were:

$$A_A = w_A + 0.5 \cdot w_{dorsal} \tag{15}$$

$$A_C = w_C + 0.5 \cdot w_{dorsal} \tag{16}$$

$$A_B = \hat{F}_x \text{ (for radial-ulnar feedback)} \tag{17}$$

IV. Evaluation

A. Experimental Setup

1) Software Implementation: We used Unity (USA, Unity Technologies) to create virtual environments and visual effects, and Springhead [29] for physics and haptic rendering. Springhead provided contact forces between rigid bodies and friction states (dynamic and static).

We used virtual coupling to connect the tracked hand position to a haptic interaction rigid body via a virtual spring. The finger bone was modeled as a capsule, and finger segments were connected using ball joints. This maintained stable interaction and produced feedback forces proportional to coupling displacement; coupling forces were obtained from the physics engine.

2) Participants: Twelve participants (8 males, 4 females; age: 22–48 years; mean = 28.0, SD = 6.7) participated, all reporting normal tactile sensitivity and no relevant neurological disorders. Participants were compensated 1000 Japanese yen. The protocol was approved by the Institute of Science Tokyo ethics committee (Approval Number: 2023362), and written informed consent was obtained. Prior experience: VR devices (occasional: 7, frequent: 3, none: 2) and haptic devices (occasional: 7, none: 5).

3) Environment and Equipment: Participants were seated at a desk in a quiet laboratory. The virtual environment was displayed on a 24-inch monitor at 60 Hz. The device was connected to a PC running Unity (2021.3.16f1) and custom haptic rendering software. A chair with adjustable height was provided to ensure that participants could maintain a natural arm position throughout the experiments. The experimental setups and corresponding interfaces are shown in Fig. 4.

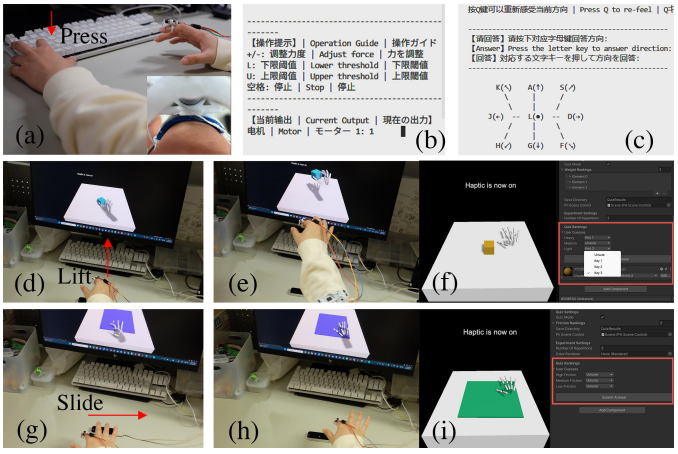

Fig. 4. Experimental setups and corresponding virtual interfaces. (a) Calibration setup: The participant wears the device and adjusts motor intensity using the keyboard with their left hand. The inset shows the Sorbothane padding for a secure fit. (b) Threshold calibration interface. (c) Direction recognition experiment interface. (d)–(f) Weight discrimination experiment: (d) Grasping gesture, (e) Lifting gesture, and (f) Virtual interface. (g)–(i) Friction discrimination experiment: (g)–(h) Lateral sliding gestures, and (i) Virtual interface.

B. Direction Recognition Experiment

We conducted a direction recognition experiment with the fingerpad suspended to avoid interference from real-world tangential forces (Fig. 4(c)).

The directional feedback system simulated virtual object movement on the fingerpad through a two-stage process. Initially, Motors A and C were set to half-maximum intensity to establish a baseline fingerpad contact pressure, while Motor B started at zero. Directional feedback was then achieved through smooth motor transitions that adjusted specific motors to represent pressure changes as objects move across the fingertip. For distal feedback, Motor C smoothly transitioned from half-intensity to maximum while Motor A simultaneously transitioned to zero, simulating forward object movement. Proximal feedback reversed this pattern. This perceived directionality arose from skin stretch dynamics at the nail wall, where proximal tension could elicit a sensation of distal movement. Radial and ulnar directions were generated by Motor B's arc-shaped pin. For the ulnar direction, the arc-shaped pin rotated to apply pressure on the finger's radial side (left side). For the radial direction, the arc-shaped pin applied pressure on the finger's ulnar side (right side), while Motors A and C maintained baseline tension. This stimulation pattern followed the natural pressure distribution when objects slide across the fingerpad, where lateral movement generates contact pressure on the opposite side of the nail wall. The dorsal direction was produced by simultaneously transitioning both Motors A and C to their maximum settings. Oblique directions combined these transition patterns. For example, the distal-ulnar direction transitioned Motor C to maximum while the arc-shaped pin applied pressure to the radial side. The distal-radial direction transitioned Motor C to maximum while the arc-shaped pin applied pressure to the ulnar side. The proximal-ulnar direction transitioned Motor A to maximum while the arc-shaped pin applied pressure to the radial side. Finally, a proximal-radial direction was created by transitioning Motor A to maximum while the arc-shaped pin applied pressure to the ulnar side. These nine directional force patterns are illustrated in Fig. 1(b).

The system generated a randomized sequence of all direction-repetition combinations to ensure an unbiased presentation order. During each trial, the system delivered feedback in one of the nine directions for a duration of 2 seconds, followed by automatic termination and no output. Each stimulus could be replayed upon request before a response was provided. Participants identified the perceived direction using designated keyboard keys mapped to the nine possible directions in a spatial layout. The system recorded the accuracy of direction identification from stimulus onset to the participant's response. All calibration parameters from the individual threshold and gain adjustment procedures were applied to ensure consistent force output across participants. Prior to the experiment, participants completed a training mode (two presentations per direction with correct answers shown). In the formal experiment, each direction was presented 5 times, resulting in a total of 45 trials across all 9 directions.

C. Weight and Friction Discrimination Experiments

To evaluate the performance of the proposed 3-DOF haptic feedback system in conveying the physical properties of virtual objects, we conducted physics-based weight and friction discrimination experiments, as shown in Fig. 4(d)–(i). The haptic

rendering methods for each condition are detailed in Section III-E. Participants were seated in front of a computer, where they could view the virtual environment on the screen. Hand pose recognition was performed by a Leap Motion controller (UK, Ultraleap) placed on the desktop. In this experiment, participants wore the proposed device on their right index finger, with no strict restrictions on their hand movements.

1) Experimental Setup and Object Configuration: Both experiments followed the same procedure and differed only in the tested physical property. Three objects were used in each experiment, with values selected using proportional spacing (Weber's law).

For the friction discrimination experiment, three cuboid objects (0.03 m × 0.03 m × 0.03 m) were configured with low, medium, and high dynamic/static friction coefficients of 0.1/0.11, 0.282/0.292, and 0.8/0.81, respectively. Participants were instructed to slide their finger across the object surface during friction assessment. Therefore, dynamic friction served as the primary tactile cue, with static friction being relevant only during the brief initial moment of contact. The small differences between static and dynamic friction coefficients represented realistic values for smooth materials such as glass, copper, and stainless steel. This design choice minimized abrupt force changes during the transition from static to dynamic friction.

For the weight discrimination experiment, three cubic objects (0.05 m × 0.05 m × 0.05 m) were assigned light, medium, and heavy masses of 10 g, 45 g, and 200 g, respectively.

2) Experimental Implementation: During the experiments, participants interacted with virtual objects, and contact forces from the physics engine were processed to generate haptic feedback. Weight differences manifested as gravitational forces during manipulation, while friction differences generated tangential resistance during sliding.

The haptic rendering approaches described in Section III-E were applied to convert these physical forces into appropriate motor commands. Force data was acquired from the Springhead physics engine, transformed to the device's local coordinate system, and processed according to the selected feedback condition. All personal calibration parameters obtained during the threshold and gain adjustment procedures were applied to ensure consistent stimulus delivery across participants.

3) Haptic Feedback Conditions: Each experiment was conducted under six distinct haptic feedback conditions. The detailed implementation of each is described in Section III-E:

1) **No Haptics**: Baseline condition with no feedback.
2) **Vibration Only**: Vibrotactile feedback during surface sliding.
3) **1-DOF Pressure**: Single-DOF feedback using total force magnitude.
4) **2-DOF No TangentX**: 2-DOF feedback via Y (distal-proximal) and Z (dorsal-ventral) axes; X (radial-ulnar) disabled.
5) **2-DOF No TangentY**: 2-DOF feedback via X (radial-ulnar) and Z (dorsal-ventral) axes; Y (distal-proximal) disabled.
6) **3-DOF Tangent**: Full 3-DOF force across all axes (X: radial-ulnar, Y: distal-proximal, Z: dorsal).

4) Object Randomization, Key Assignment, and Interaction Protocol: At the start of each session, the three test objects were randomly mapped to keys 1–3 to reduce learning bias. Pressing a key spawned only the corresponding object. For logging, each object was assigned an invisible color tag. Threshold and gain values from calibration were applied.

Participants used their right index finger to: (1) spawn objects via keys 1–3; (2) lift objects gently without shaking (weight) or slide to feel resistance (friction); and (3) repeat for comparison.

After exploration, they ranked the objects using the same keys (Heavy/Medium/Light or High/Medium/Low friction). Rankings could be left blank when uncertain.

To counterbalance order effects, the six haptic-feedback conditions were presented in a random sequence. Each condition was repeated three times per experiment, for a total of 18 runs. The system logged all feedback settings and interaction data.

D. Friction Discrimination with Physical Contact

To test robustness under physical contact, an additional friction discrimination experiment was conducted with the fingerpad in contact with a physical surface.

1) Participants: A separate group of 12 participants (10 males, 2 females, age range: 22–49 years, mean = 27.0, SD = 7.4) was recruited for this supplementary experiment. Recruitment, compensation, ethical approval, and calibration procedures followed those in Section IV-A2. Prior experience with VR and haptic devices was not collected, as this experiment focused on validating device performance under physical contact rather than experience-dependent effects.

2) Experimental Setup: The experimental setup was modified to include a physical surface, as shown in Fig. 5. A transparent acrylic plate was positioned horizontally to serve as the physical interaction surface. Unlike the previous experiments where the hand tracker was placed on the desktop, here the Leap Motion Controller was mounted overhead, facing downwards. This configuration minimized occlusion issues caused by the hand covering the tracker while interacting with the physical plate (Fig. 5(b)).

Participants were instructed to keep their right index finger in contact with the acrylic plate while sliding it laterally to perceive the virtual friction. To ensure consistent normal force application and prevent excessive pressure that could mask the device's haptic feedback, a reference object (6 cm × 6 cm × 3 cm, 140 g) was prepared to represent a moderate contact pressure. Before the experiment, the experimenter demonstrated the appropriate contact force by placing the reference object on the plate, and participants were instructed to maintain similar pressure during sliding. The left hand was used to operate a keyboard to switch between different friction coefficients (High, Medium, Low) for comparison. These levels corresponded to the same kinetic friction coefficients used in the previous experiment ($\mu_k \in \{0.1, 0.282, 0.8\}$). The system was aligned such that when the participant's physical fingertip touched the acrylic plate, the virtual fingertip penetrated the virtual surface by approximately 10 mm. This

penetration depth was selected to maintain consistent virtual coupling forces: smaller depths would result in insufficient force generation.

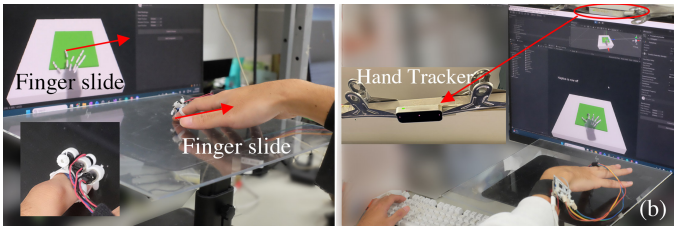

Fig. 5. Experimental setup for friction discrimination with physical contact. (a) The participant slides their index finger on a transparent acrylic plate (sliding element) while receiving virtual friction feedback. (b) Overall setup: The hand tracker is positioned overhead to minimize occlusion. The participant uses their left hand to switch between varying friction coefficients using the keyboard.

3) Conditions: We compared four conditions to evaluate the robustness of the feedback:

1) **3-DOF Tan (No Contact)**: The standard condition from the previous experiment (suspended finger).
2) **3-DOF Tan (With Contact)**: The proposed method applied while the user touched the physical acrylic plate.
3) **2-DOF (No X)**: Tangential feedback without the radial-ulnar component.
4) **2-DOF (No Y)**: Tangential feedback without the distal-proximal component.

E. Subjective Evaluation

Following all experimental tasks, participants independently completed a multilingual questionnaire (available in English, Japanese, and Chinese) to minimize experimenter bias. The questionnaire first assessed their background experience with VR and haptic devices (none, occasional, frequent). It then used a 7-point Likert scale (1=Strongly disagree, 7=Strongly agree) to evaluate two main areas. First, a general assessment of the device covered comfort, interference with real objects, ease of use, responsiveness, and overall satisfaction. Second, for each primary haptic condition (1-DOF, Vibration, and 3-DOF), it assessed feedback clarity, perceived accuracy for conveying weight and friction, fatigue, and overall interaction satisfaction.

V. Results

A. Direction Recognition Performance

Fig. 6 shows the direction-recognition confusion matrix (nine directions) for the 3-DOF nail wall-based device across all participants.

1) Overall Accuracy: The system achieved an overall accuracy of 63.52% across all nine directions and 540 total trials (60 trials per direction), exceeding random chance (11.11%) but leaving room for improvement.

2) Per-Direction Performance Analysis: Performance varied across different directions, with certain directions showing higher recognition rates than others. The highest-performing directions included proximal-radial, with 73% precision and

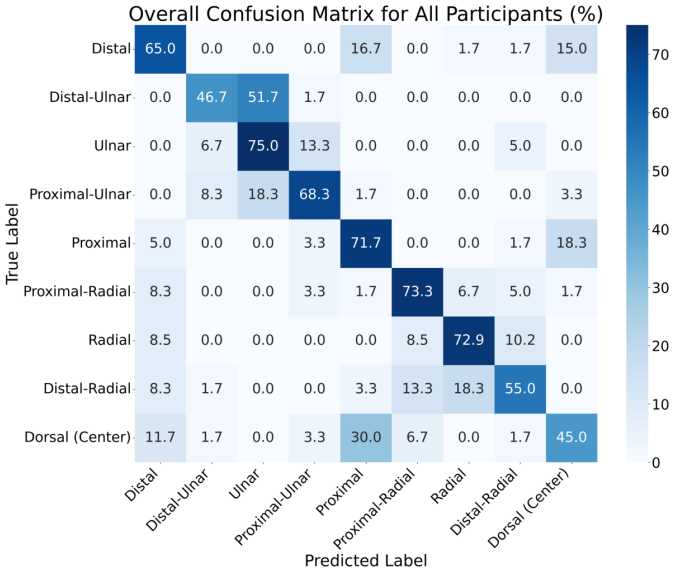

Fig. 6. Overall confusion matrix (recall rates) for direction recognition experiment. The matrix shows the classification performance across all nine directions, with darker blue indicating higher accuracy rates. Diagonal elements represent correct classifications, while off-diagonal elements show confusion patterns between different directions.

73% recall (F1-score: 0.73); radial, with 73% precision and 72% recall (F1-score: 0.72); and proximal-ulnar, with 73% precision and 68% recall (F1-score: 0.71). These results indicated that the combination of string-based and pin-based actuation conveyed directional information for oblique and pure radial/ulnar directions.

Moderate performance was observed for the proximal (57% precision, 72% recall, F1-score: 0.64), distal (61% precision, 65% recall, F1-score: 0.63), ulnar (52% precision, 75% recall, F1-score: 0.61), and distal-radial (69% precision, 55% recall, F1-score: 0.61) directions. The moderate performance for pure distal and proximal directions suggested that while participants could detect these stimuli, the string-based actuation may have been less distinctive compared to the pin-based radial/ulnar feedback.

The most challenging directions were distal-ulnar, with 72% precision and 47% recall (F1-score: 0.57), and dorsal center, with 54% precision and 45% recall (F1-score: 0.49). The dorsal direction, created by the simultaneous activation of both string motors, showed the lowest performance, with only 45% of stimuli correctly identified, suggesting that the combined string tension may not have created a sufficiently distinct sensation compared to the individual directional cues.

B. Weight Discrimination Performance

Figs. 7 and 8 summarize weight discrimination across three masses and six haptic feedback conditions.

1) Overall Performance Comparison: Vibration-only feedback achieved the highest overall accuracy at 54% (SD = 39.59%), followed closely by the 3-DOF tangential feedback at 52% (SD = 35.87%). The 2-DOF configurations showed moderate performance: 2-DOF No TangentX achieved 44% accuracy (SD = 36.53%), and 2-DOF No TangentY achieved

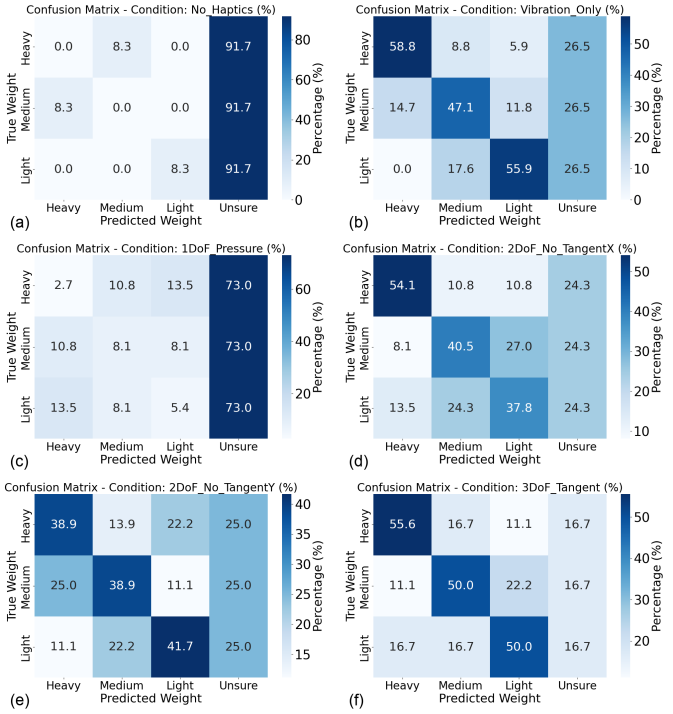

Fig. 7. Weight discrimination confusion matrices (recall rates) across all haptic feedback conditions. Each subplot shows the classification performance for different weight categories (Heavy: 200 g, Medium: 45 g, Light: 10 g) under six experimental conditions: (a) No Haptics; (b) Vibration Only; (c) 1-DOF Pressure; (d) 2-DOF No TangentX; (e) 2-DOF No TangentY; and (f) 3-DOF Tangent. Darker blue indicates higher accuracy rates, with "Unsure" responses shown in the rightmost column.

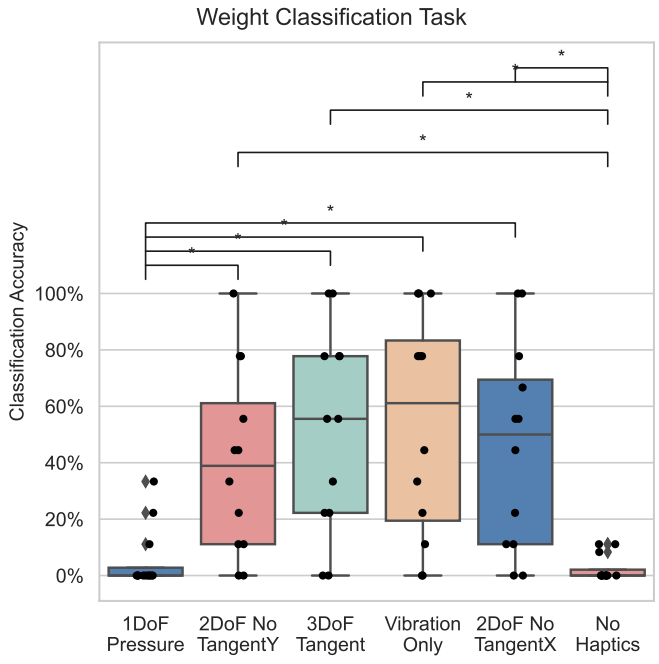

Fig. 8. Statistical comparison of weight discrimination performance across haptic feedback conditions. The box plots show the distribution of accuracy scores for each condition, with individual participant data points overlaid. The 3-DOF tangential feedback and vibration-only conditions achieved the highest performance, significantly outperforming single-dimensional approaches. The accuracy scores include "Unsure" responses, which are treated as incorrect judgments to reflect participants' confidence levels in the discrimination tasks. (* indicates $p < 0.05$, ** indicates $p < 0.01$).

40% accuracy (SD = 32.98%). Single-degree-of-freedom pressure feedback performed poorly, with only 5% accuracy (SD = 11.11%), while the no-haptics control condition achieved minimal performance at 3% accuracy (SD = 4.66%).

2) Statistical Analysis: A Friedman test revealed significant overall differences between conditions (χ^2 = 35.99, p < 0.001). Post-hoc pairwise comparisons with Holm correction identified several significant differences. The 1-DOF pressure condition performed significantly worse than all multi-dimensional feedback approaches: 2-DOF No TangentY ($p < 0.05$), 3-DOF Tangent ($p < 0.01$), Vibration Only ($p < 0.01$), and 2-DOF No TangentX ($p < 0.01$). All haptic feedback conditions significantly outperformed the no-haptics control (all $p < 0.01$), demonstrating the benefit of haptic information for weight perception.

3) Condition-Specific Performance Analysis: The vibration-only condition showed the most balanced performance across the weight categories. Heavy objects achieved 59% recall, medium objects 47% recall, and light objects 56% recall. The precision values were correspondingly high at 80%, 64%, and 76% respectively, indicating that when participants identified objects in these categories, they were generally correct.

The 3-DOF tangential feedback condition demonstrated consistent performance across all weight categories, with recall rates of 56% for heavy objects, 50% for medium objects, and 50% for light objects. The precision values (67%, 60%, and 60% respectively) suggest reliable discrimination capabilities when directional force information was available.

The 2-DOF conditions showed intermediate performance. 2-DOF No TangentX achieved better heavy object discrimination (54% recall, 71% precision) compared to 2-DOF No TangentY (39% recall, 52% precision), suggesting that the specific axes of tangential feedback influenced weight perception capabilities.

4) Uncertainty Analysis: Participants' uncertainty levels, as measured by "Unsure" responses, varied across conditions. The no-haptics condition resulted in 92% uncertain responses, while 1-DOF pressure feedback led to 73% uncertainty. In contrast, the 3-DOF tangential feedback achieved the lowest uncertainty rate at 17

C. Friction Discrimination Performance

Figs. 9 and 10 summarize friction discrimination across three friction coefficients and six haptic feedback conditions.

1) Overall Performance Comparison: The 3-DOF tangential feedback achieved the highest overall accuracy at 79% (SD = 20.36%), closely matched by vibration-only feedback at 79% (SD = 27.42%). The 2-DOF configurations also showed good performance: 2-DOF No TangentY achieved 75% accuracy (SD = 26.00%), and 2-DOF No TangentX achieved 72% accuracy (SD = 24.83%). Single-degree-of-freedom pressure feedback performed poorly, with only 13% accuracy (SD = 29.76%), while the no-haptics control condition achieved minimal performance at 14% accuracy (SD = 29.59%).

2) Statistical Analysis: A Friedman test revealed highly significant overall differences between conditions ($\chi^2 = 41.82$,

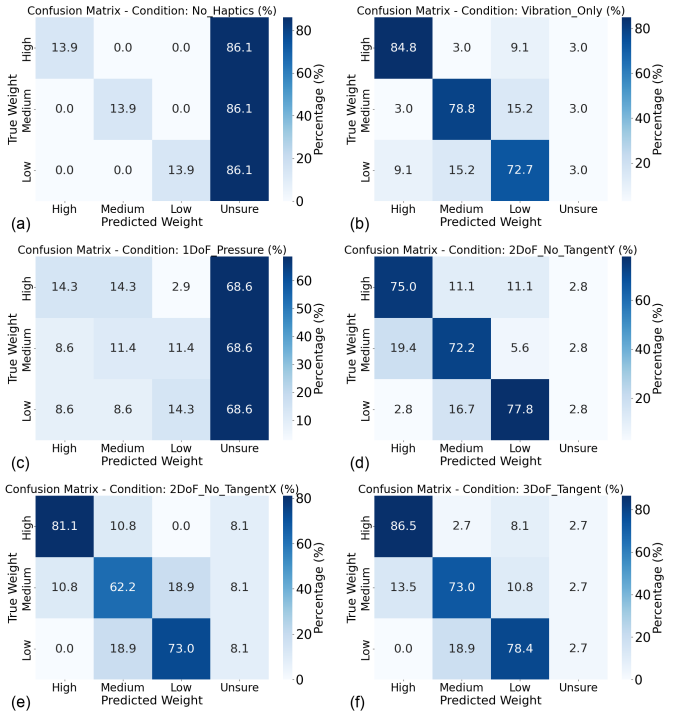

Fig. 9. Friction discrimination confusion matrices (recall rates) across all haptic feedback conditions. Each subplot shows the classification performance for different friction categories (High: μ = 0.8, Medium: μ = 0.282, Low: μ = 0.1) under six experimental conditions: (a) 3-DOF Tangent; (b) 1-DOF Pressure; (c) 2-DOF No TangentX; (d) Vibration Only; (e) 2-DOF No TangentY; and (f) No Haptics. Darker blue indicates higher accuracy rates, with "Unsure" responses shown in the rightmost column.

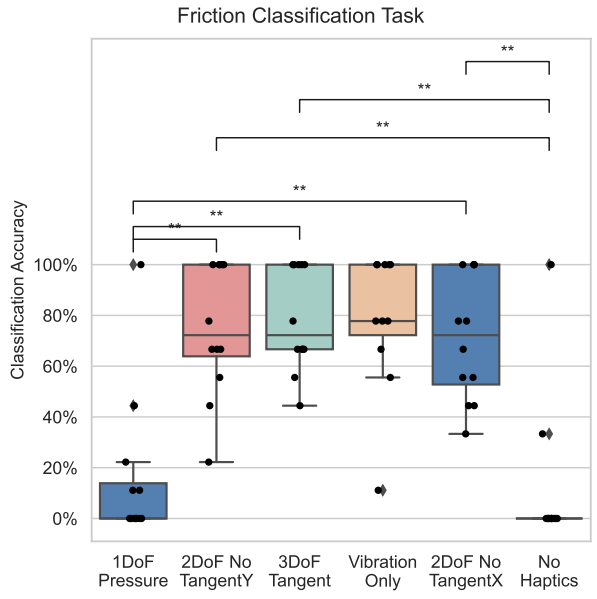

Fig. 10. Statistical comparison of friction discrimination performance across haptic feedback conditions. The box plots show the distribution of accuracy scores for each condition, with individual participant data points overlaid. The 3-DOF tangential feedback and vibration-only conditions achieved the highest performance, significantly outperforming single-dimensional approaches. The accuracy scores include "Unsure" responses, which are treated as incorrect judgments to reflect participants' confidence levels in the discrimination tasks.

$p < 0.001$). Post-hoc pairwise comparisons with Holm correction identified several significant differences. The 1-DOF pressure condition performed significantly worse than all multi-dimensional feedback approaches: 2-DOF No TangentY ($p < 0.01$), 3-DOF Tangent ($p < 0.01$), and 2-DOF No TangentX ($p < 0.01$). All multi-dimensional haptic feedback conditions significantly outperformed the no-haptics control: 2-DOF No TangentY vs No Haptics ($p < 0.01$), 3-DOF Tangent vs No Haptics ($p < 0.01$), and 2-DOF No TangentX vs No Haptics ($p < 0.01$). No significant differences were found between the multi-dimensional feedback conditions themselves, indicating their comparable performance.

Note that although the no-haptics condition achieved only 14% overall accuracy, a few individual data points in Fig. 10 show high accuracy. These outliers arose because the experiment imposed no time limit for exploration, and a small number of participants discovered they could infer friction levels by observing subtle differences in the virtual finger's physical behavior (e.g., stick-slip artifacts in the physics engine). These isolated cases do not affect the overall conclusion, as the median no-haptics performance remained near chance level.

3) Condition-Specific Performance Analysis: The 3-DOF tangential feedback condition demonstrated better and balanced performance across all friction categories. High-friction objects achieved 86% recall with 86% precision (F1-score: 0.86). Medium-friction objects achieved 73% recall with 77% precision (F1-score: 0.75). Low-friction objects achieved 78% recall with 81% precision (F1-score: 0.79). This consistent performance across friction levels indicated that directional force information conveyed surface texture differences.

The vibration-only condition showed similarly strong performance. High-friction objects achieved 85% recall and 88% precision (F1-score: 0.86). Medium-friction objects achieved 79% recall and 81% precision (F1-score: 0.80). Low-friction objects achieved 73% recall and 75% precision (F1-score: 0.74), indicating that dynamics from surface contact variations provided reliable cues for friction discrimination.

The 2-DOF conditions showed good but slightly reduced performance compared to the full 3-DOF system. 2-DOF No TangentY achieved 75% recall for high-friction objects (77% precision), while 2-DOF No TangentX achieved 81% recall for high-friction objects (88% precision). The performance difference between these two 2-DOF configurations suggested that specific axes of tangential feedback contributed differently to friction perception.

4) Uncertainty Analysis: Participants' uncertainty levels varied across conditions, mirroring the results of the weight discrimination experiment. The no-haptics condition resulted in 86% uncertain responses, while 1-DOF pressure feedback led to 69% uncertainty. In contrast, the 3-DOF tangential feedback achieved the lowest uncertainty rate at only 3

5) Comparison with Weight Discrimination: Friction discrimination performance was higher than weight discrimination performance across all multi-dimensional feedback conditions. The 3-DOF tangential feedback achieved 79% accuracy for friction versus 52% for weight, while vibration feedback achieved 79% for friction versus 54% for weight, suggesting

that surface texture information may be more easily conveyed through haptic feedback than gravitational or inertial cues.

D. Friction Perception under Physical Contact

Fig. 11 compares friction classification accuracy across the tested conditions under physical contact.

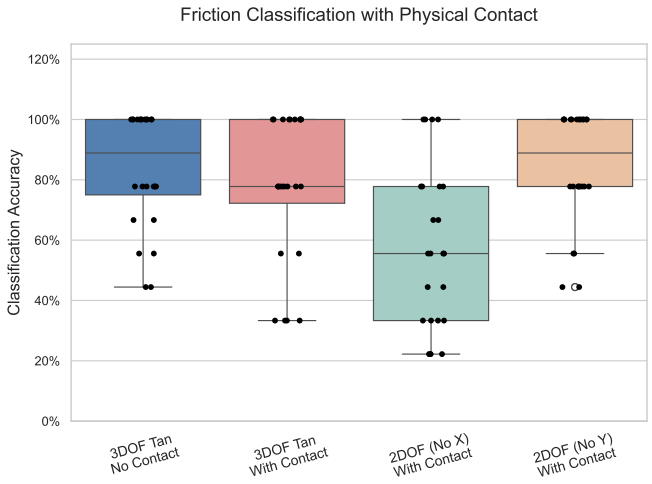

Fig. 11. Friction classification accuracy comparison between non-contact and physical contact conditions. The 3-DOF tangential feedback maintained high accuracy even with physical contact.

A Friedman test indicated a significant difference in performance among the conditions ($\chi^2(3) = 10.375, p = 0.0156$). Post-hoc analysis with Holm correction revealed a significant difference between the *3-DOF Tan (No Contact)* and *2-DOF (No X)* conditions ($p = 0.0410$).

There was no significant difference observed between the *3-DOF Tan (No Contact)* and *3-DOF Tan (With Contact)* conditions. The median accuracy for the physical contact condition remained high (approx. 80%), comparable to the non-contact baseline. This finding supports the hypothesis that the proposed nail wall-based stimulation remains effective even when fingerpad mechanoreceptors are saturated by physical contact pressure. Although the significant difference between *3-DOF Tan (No Contact)* and *2-DOF (No X)* suggests that the physical surface might have slightly influenced the perception of lateral force cues (likely due to friction masking), the overall high accuracy confirms that the device superimposed directional friction cues onto the constant physical sensation of the acrylic plate.

E. Subjective Evaluation Results

Following the completion of all experimental tasks, participants completed a subjective evaluation questionnaire to assess their experience with the haptic feedback device under different conditions. To minimize experimenter bias, they filled it out independently. The questionnaire used a 7-point Likert scale (1 = Strongly disagree, 7 = Strongly agree) to assess general device usability (Q1-Q5) and the user experience for the 1-DOF, Vibration, and 3-DOF feedback conditions (Q6-Q9).

TABLE I
GENERAL DEVICE ASSESSMENT RESULTS (7-POINT LIKERT SCALE)

Question	Median	IQR
Q1: The device was comfortable to wear.	5.0	1.50
Q2: The device minimally interfered with real object manipulation.	6.0	1.00
Q3: The device was easy to operate and adjust.	5.0	0.50
Q4: The device had a quick response and timely feedback.	6.5	1.00
Q5: I was satisfied with the overall device performance.	5.5	1.00

1) General Device Assessment (Q1-Q5): Participants evaluated the device's general usability across five criteria, with the results summarized in Table I. The device received high ratings for responsiveness (Q4, Median = 6.5) and for minimal interference with real object manipulation (Q2, Median = 6.0). Overall satisfaction (Q5, Median = 5.5) and ease of operation (Q3, Median = 5.0) were also rated positively. Device comfort (Q1, Median = 5.0) was deemed acceptable, though this indicated potential for future ergonomic improvements.

2) Condition-Specific User Experience (Q6-Q9): Participants evaluated feedback clarity (Q6), accuracy (Q7), fatigue (Q8), and overall satisfaction (Q9) across the three main haptic conditions. While 3-DOF feedback was rated as the clearest (Q6: M = 5.67), the trend did not reach statistical significance ($\chi^2 = 4.15, p>0.05$). Significant differences emerged in perceived accuracy (Q7: $\chi^2 = 15.76, p<0.001$). Both 3-DOF (M = 5.75) and vibration feedback (M = 5.50) were rated as significantly more accurate than the 1-DOF condition (M = 2.33, $p<0.01$). Regarding fatigue (Q8), all conditions were rated as comfortable for extended use, with no significant differences. Crucially, overall interaction satisfaction (Q9) varied significantly ($\chi^2 = 11.23, p<0.01$). The 3-DOF feedback (M = 5.58) achieved significantly higher satisfaction ratings than both the 1-DOF (M = 3.75, $p<0.01$) and vibration-only feedback (M = 4.08, $p<0.05$), highlighting its better user experience.

VI. DISCUSSION

A. Direction Recognition Experiment

The direction recognition results, with an overall accuracy of 63.52%, demonstrated that participants could reliably distinguish between nine distinct haptic patterns delivered through nail wall stimulation. This outperformed random chance (11.11%). While the specific mapping between stimulus locations and perceived sliding directions represented a learned association rather than an intuitive correspondence, the main finding was that each pattern elicited a sufficiently distinct sensation to enable discrimination.

The systematic performance differences across directions reflected the underlying actuation mechanisms and human tactile sensitivity patterns. Pin-based radial-ulnar feedback achieved higher accuracy (72-75% recall) due to its localized pressure concentration, which consistently activates specific mechanoreceptor populations. In contrast, string-based distal-proximal feedback showed moderate performance (65-72%

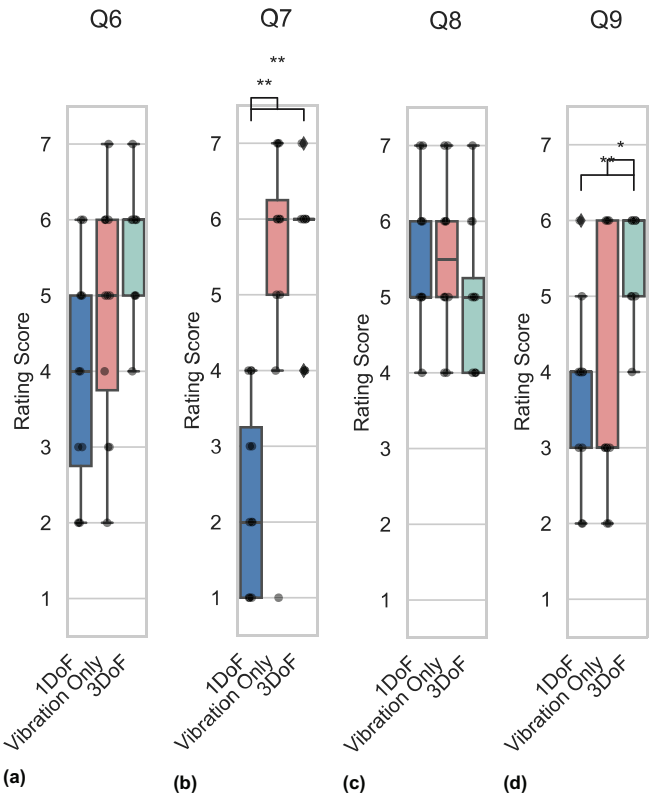

Fig. 12. Subjective evaluation results across haptic feedback conditions. The box plots show participant ratings on a 7-point Likert scale for four evaluation criteria: (Q6) Feedback clarity and distinctiveness, (Q7) Accuracy of physical property conveyance, (Q8) Extended use fatigue assessment, and (Q9) Overall interaction satisfaction. Individual participant responses are overlaid as points.

recall). This approach faced perceptual challenges related to the lower density of directionally-sensitive mechanoreceptors in the proximal nail wall area and the inherent difficulty in discriminating between opposing directional stimuli applied through similar anatomical pathways.

The confusion patterns revealed both perceptual and mechanical factors. Distal stimuli were frequently confused with proximal directions (30% of cases), which is attributed to the perceptual ambiguity of skin stretch; the physical direction of string tension does not always align with the perceived direction of motion. The dorsal direction (45% recall) proved to be the most challenging, as the simultaneous activation of both strings failed to create a perceptually distinct "center" sensation for many participants.

The consistently high precision values (69-73%) across most directions indicated that when participants correctly identified a direction, their responses were reliable. The mean angular error of 22.40° with a median of 0° suggested that most misclassifications involved adjacent rather than random directions, supporting the systematic nature of the discrimination capability.

These results established the feasibility of using standardized nail wall devices for directional feedback without individual customization, despite inherent variability in hand anatomy and tactile sensitivity. While extended training might improve absolute accuracy, the demonstrated ability to distinguish nine distinct patterns provides sufficient information bandwidth for multi-dimensional haptic applications.

B. Weight and Friction Perception

Performance Gap Between Tasks. The significant performance gap between friction recognition (79% in 3-DOF) and weight recognition (52% in 3-DOF) revealed fundamental differences in how these properties are conveyed through spatial versus temporal haptic mechanisms. Friction information is primarily conveyed through spatial directional forces that directly activate directionally-sensitive mechanoreceptors around the nail border through spatially-organized stimulation. In contrast, weight perception relies on gravitational and inertial cues that manifest as static force magnitudes. These cues are more difficult to convey through the nail wall interface.

Vibrotactile Feedback Performance. Vibrotactile feedback achieved moderate performance (54% for weight, 79% for friction) through temporal mechanisms that differ fundamentally from spatial force feedback. For friction tasks, vibration conveys surface texture through temporal dynamics during sliding contact. However, in weight discrimination, the apparent performance was largely an artifact of physics engine limitations. Calculation errors prevented stable static grasping, resulting in continuous micro-sliding (measured relative velocity: 2.88 $\pm$ 0.88 mm/s during intended static grasping). Participants discriminated based on vibration intensity rather than intuitive force perception. This artifact represents a limitation of the current study's implementation. Future work should prioritize rigorous validation of the physics engine's stability to ensure that static contact is reliably maintained before conducting similar experiments. A key limitation of vibrotactile feedback is that it only works during sliding motion. Without sliding, there is no vibration, and thus no tactile information can be perceived. This limits its use in static contact situations where directional force information is still needed.

Kinetic vs. Static Friction. The friction discrimination experiment focused on kinetic friction during sliding contact. Static friction discrimination presents different perceptual challenges, as it relies primarily on tangential force buildup before the onset of slip rather than on surface texture dynamics. Research by Johansson and Westling [30] demonstrated that humans can detect incipient slip through tactile sensors that respond to tangential skin deformation before gross sliding occurs. Partial slip phenomena, where contact transitions from static to kinetic friction at the contact periphery while maintaining static contact at the center, provide additional tactile cues for friction assessment [31]. The ability of the proposed 3-DOF system to convey directional tangential forces suggests its potential applicability to static friction discrimination by detecting force magnitude at the slip threshold, though this requires dedicated experimental validation.

Advantages of 3-DOF Over Vibration. Despite comparable performance data, the proposed 3-DOF system offers critical advantages through spatial directional stimulation rather than temporal vibration. While vibration conveys surface texture through temporal dynamics, directional stimulation provides spatial force vector information. This enables the perception

of contact forces, friction directions, and gravitational effects during both static and dynamic interactions. Key advantages of 3-DOF over vibration include: (1) significantly higher user satisfaction (M = 5.58 vs 4.08, $p < 0.05$), (2) lower uncertainty in weight discrimination (17% vs 26% "Unsure" responses), and (3) functional capability during static contact, where vibration provides no information. These benefits demonstrate that while accuracy may be comparable, the 3-DOF system provides a better user experience and broader applicability for haptic interaction scenarios.

Interpretation of Non-Significant Differences. While the 3-DOF condition did not show a statistically significant performance advantage over the 2-DOF and vibration conditions in the friction task, this result itself offers an insight. It suggests that for perceiving kinetic friction, which primarily manifests as resistance along the direction of motion, a single channel of tangential or temporal feedback may be sufficient to reach a performance plateau. The addition of a second tangential force channel (in the 3-DOF condition) may not provide additive information for this specific task, as the dominant cues are already captured by one dimension of feedback. However, we re-emphasize that despite the comparable accuracy, the 3-DOF condition achieved significantly higher user satisfaction ratings, indicating that the richer, multi-dimensional feedback created a more intuitive and preferred user experience, even if it did not translate to higher task scores.

Limitations of 1-DOF Pressure Feedback. The 1-DOF pressure feedback showed poor performance (5% for weight, 13% for friction), indicating that force magnitude alone, without spatial directional information or temporal dynamics, could not convey physical properties. Although the 1-DOF system represented the total force magnitude, which should theoretically distinguish different weights, the weight-related gravitational components were overwhelmed by the larger tangential force components during object manipulation. This masking effect occurred because virtual object interaction generated lateral and normal forces (typically 0.5–2.0 N) that dwarfed the subtle gravitational force differences between objects (maximum 0.2 N difference). The 1-DOF system integrated all force components into a single magnitude value. This made the small weight-related signals indistinguishable within the larger force envelope created by contact and manipulation forces. This masking effect demonstrated that effective property discrimination required either spatial directional channels (as in the proposed 3-DOF system) or temporal dynamic patterns (as in vibrotactile feedback), rather than simple magnitude information.

C. Device Usability and User Experience

The subjective evaluation results confirmed the practical viability of the proposed nail wall-based haptic feedback approach. The device's high ratings for responsiveness and minimal interference with real-world objects validated the core design goal of preserving natural fingertip sensation for mixed reality applications. While participants rated the device as easy to operate and generally comfortable, the moderate comfort scores suggested that ergonomic design is an area for future improvement. A detailed comparison of the haptic conditions provided further insights into user preferences beyond objective task performance. Participants perceived the 3-DOF feedback as more accurate in conveying physical properties than the 1-DOF approach. This aligned with the objective discrimination results and confirmed that force magnitude alone is insufficient.

The richer feedback of the 3-DOF system did not lead to increased user fatigue compared to simpler modalities. The 3-DOF feedback achieved higher overall interaction satisfaction than both vibration-only and 1-DOF feedback, suggesting that even when objective performance is comparable, as in the friction task, the spatial and directional nature of the 3-DOF feedback created a more intuitive user experience.

D. Comparison with State-of-the-Art

Table II compares the proposed device with both classic and state-of-the-art (2025) wearable fingertip interfaces.

Evolution of Nail-Mounted Haptics. Early nail-mounted devices [5] and recent iterations like PhantomFolds (2025) [6] preserve fingerpad sensitivity but are limited to vibrotactile feedback. While effective for texture, they cannot render the static directional forces required for weight or grasping.

Force Feedback Trade-offs. Traditional devices (e.g., [9]) use rigid platforms that add significant weight (>30 g) and often occlude the fingerpad. While recent lightweight solutions like StringTouch (2025) [13] also use strings, they employ rigid guide structures along the finger sides. These protrusions physically obstruct finger adduction (closing fingers together), thereby hindering natural inter-finger manipulation. In contrast, the proposed device concentrates components around the nail, minimizing lateral protrusion to allow more natural hand dexterity. By combining tendons for distal-proximal forces and an arc-pin for lateral support, it achieves distinct 3-DOF directionality. However, this hybrid approach introduces an inherent asymmetry: lateral forces are concentrated at a specific pin contact point, while distal-proximal forces are distributed along the string path. Additionally, the proximal actuator placement presents mounting challenges that currently limit the maximum output force for distal feedback compared to the robust lateral pin mechanism.

E. Limitations and Future Work

The accuracy of direction recognition (63.52%) and weight discrimination (52%), while exceeding random chance, indicates room for improvement before deployment in precision-critical tasks. This currently limits its use to exploratory or assistive contexts. The system achieved higher performance in friction discrimination (79% accuracy) compared to weight and direction recognition tasks. These limitations stemmed from several technical factors. The string-based distal-proximal feedback mechanism faced perceptual challenges due to the asymmetric distribution of mechanoreceptors around the nail border, with proximal areas exhibiting lower tactile sensitivity than the lateral borders. Additionally, Motor C's reduced force output (0.29 N compared to Motor A's

TABLE II
COMPARISON WITH STATE-OF-THE-ART WEARABLE FINGERTIP DEVICES

Device [Ref]	Year	DOF	Weight	Fingerpad	Key Capabilities & Limitations
Messerschmidt [6]	2025	-	$\approx$ 5 g	Open	**Cap:** Unobtrusive spatial vibration on nail. **Lim:** Vibrotactile only; no static force.
StringTouch [13]	2025	3	Light	Open	**Cap:** 3-DOF skin deformation via strings. **Lim:** Rigid side guides; hinders finger adduction.
HydroRing [8]	2018	1	$<$ 5 g	Open	**Cap:** Pressure & thermal feedback. **Lim:** Normal force only; fluid latency.
Prattichizzo [9]	2013	3	$\approx$ 30 g	Occluded	**Cap:** High-fidelity force vector at fingertip. **Lim:** Obstructs fingerpad; bulky structure.
Proposed Device	**2025**	**3**	**5.24 g**	**Open**	**Cap:** Hybrid (Pin+String) nail wall stimulation. **Lim:** Asymmetric point/line actuation; mounting limits.

1.38 N) due to mechanical constraints in the proximal mounting position contributed to weaker distal directional feedback, requiring future optimization of the actuation mechanism. Overlapping receptive fields between stimulation sites created directional confusion. This particularly affected dorsal direction recognition (45% accuracy), where simultaneous string activation failed to create a perceptually distinct sensation for many participants.

Future weight discrimination studies could benefit from additional measurements to better understand the underlying mechanisms. Collecting grasp force data and finger distance measurements during virtual object manipulation would provide insights into how participants adapt their gripping strategies in response to perceived weight differences. This could potentially reveal whether the proposed haptic feedback triggered natural weight-related motor responses.

Additionally, while this study prioritized evaluating the feasibility of the proposed method using categorical stimuli, future work should investigate performance when weight and friction cues are parametrically varied. Examining the perception of continuous changes in these properties will provide deeper insights into the device's psychophysical resolution.

If an application focuses on texture and surface property recognition, a simplified 2-DOF system may be sufficient. This would reduce system complexity while maintaining performance. However, for physical property recognition, including weight perception, a full 3-DOF feedback system is required. In the future, we will focus on using small actuators that specifically stimulate mechanoreceptors on the side of the fingernail to generate tangential force sensations.

Finally, the device's fixed-size design limits broad applicability. Although manually adjusted Sorbothane padding accommodated the participants, this ad-hoc approach lacks the systematic adaptability required for personalized devices. Research has shown that compensating for fingertip size improves tactile accuracy [32] and personalized interfaces accounting for morphology enhance both comfort and effectiveness [33]. Future work should incorporate adjustable mechanisms for broader applicability.

VII. CONCLUSION

This paper addressed the fundamental trade-off between rich tactile feedback and preserved dexterity. We developed and validated a 3-DOF nail wall-based haptic device that delivered directional force feedback without obstructing the fingerpad. This approach was proven effective through experiments where users performed object property discrimination tasks, confirming that nail wall stimulation is a viable channel for complex haptic information while maintaining natural interaction capabilities.

The experimental evaluation demonstrated that exploiting mechanoreceptors around the nail border for haptic feedback is viable. The 3-DOF system showed improvements over single-dimensional approaches in both weight and friction discrimination tasks. Future work will focus on improving this directional fidelity. Potential solutions include enhancing the mechanical design by incorporating a third actuation point to create a more localized and distinct dorsal stimulus.

This research provides several insights for future haptic device development. First, the performance of mechanical-based nail wall stimulation demonstrates that alternative anatomical targets beyond the fingerpad can provide effective haptic channels while preserving natural dexterous capabilities. This opens new design possibilities for wearable haptic interfaces that require minimal interference with daily activities. Second, these findings revealed that friction information is more readily conveyed through directional force feedback than weight information, suggesting that different physical properties may require tailored haptic rendering strategies.

REFERENCES

[1] R. S. Johansson, U. Landstro, R. Lundstro *et al.*, "Responses of mechanoreceptive afferent units in the glabrous skin of the human hand to sinusoidal skin displacements," *Brain research*, vol. 244, no. 1, pp. 17–25, 1982.

[2] K. O. Johnson, "The roles and functions of cutaneous mechanoreceptors," *Current opinion in neurobiology*, vol. 11, no. 4, pp. 455–461, 2001.

[3] I. Birznieks, V. G. Macefield, G. Westling, and R. S. Johansson, "Slowly adapting mechanoreceptors in the borders of the human fingernail encode fingertip forces," *Journal of Neuroscience*, vol. 29, no. 29, pp. 9370–9379, 2009.

[4] A. Tamura and S. Okamoto, "Richer textural information in the horizontal component of the contact force compared with the normal component," in *2024 IEEE Haptics Symposium (HAPTICS)*. IEEE, 2024, pp. 13–18.

[5] H. Ando, J. Watanabe, M. Inami, M. Sugimito, and T. Maeda, "A fingernail-mounted tactile display for augmented reality systems," *Electronics and Communications in Japan (Part II: Electronics)*, vol. 90, no. 4, pp. 56–65, 2007.

[6] M. A. Messerschmidt, D. J. Matthies, P. Sasikumar, and S. Nanayakkara, "Phantomfolds: Exploring unobtrusive spatial tactile feedback produced by two fingernail mounted lras for in-air and on-surface mixed reality applications," *International Journal of Human–Computer Interaction*, pp. 1–27, 2025.

[7] T. Aoki, H. Mitake, D. Keoki, S. Hasegawa, and M. Sato, "Wearable haptic device to present contact sensation based on cutaneous sensation using thin wire," in *Proceedings of the International Conference on Advances in Computer Entertainment Technology*, 2009, pp. 115–122.

[8] T. Han, F. Anderson, P. Irani, and T. Grossman, "Hydroring: Supporting mixed reality haptics using liquid flow," in *Proceedings of the 31st Annual ACM Symposium on User Interface Software and Technology*, 2018, pp. 913–925.

[9] D. Prattichizzo, F. Chinello, C. Pacchierotti, and M. Malvezzi, "Towards wearability in fingertip haptics: a 3-dof wearable device for cutaneous force feedback," *IEEE Transactions on Haptics*, vol. 6, no. 4, pp. 506–516, 2013.

[10] F. Chinello, M. Malvezzi, C. Pacchierotti, and D. Prattichizzo, "Design and development of a 3rrs wearable fingertip cutaneous device," in *2015 IEEE International Conference on Advanced Intelligent Mechatronics (AIM)*. IEEE, 2015, pp. 293–298.

[11] D. Tsetserukou, S. Hosokawa, and K. Terashima, "Linktouch: A wearable haptic device with five-bar linkage mechanism for presentation of two-dof force feedback at the fingerpad," in *2014 IEEE Haptics Symposium (HAPTICS)*. IEEE, 2014, pp. 307–312.

[12] V. Yem and H. Kajimoto, "Wearable tactile device using mechanical and electrical stimulation for fingertip interaction with virtual world," in *2017 IEEE Virtual Reality (VR)*. IEEE, 2017, pp. 99–104.

[13] Y. Kim, J. Yim, Y. Yun, D. Ko, and G. Lee, "Stringtouch: A non-occlusive 3dof haptic interface using string structures for modulating finger sensations," in *Proceedings of the 38th Annual ACM Symposium on User Interface Software and Technology*, 2025, pp. 1–14.

[14] S. Nakayama, K. Ushiyama, and H. Kajimoto, "Force cue presentation by electrical stimulation to lateral side of the finger."

[15] J. E. Palmer, B. B. Vuong, Z. Zhakypov, Y. Qin, L. Tilton, and A. M. Okamura, "Haptic relocation of virtual finger forces via pneumatic wrist-worn haptic devices," in *2024 IEEE Haptics Symposium (HAPTICS)*. IEEE, 2024, pp. 315–320.

[16] T. Moriyama, T. Nakamura, and H. Kajimoto, "Development of a wearable haptic device that presents the haptic sensation corresponding to three fingers on the forearm," in *Proceedings of the 2018 ACM Symposium on Spatial User Interaction*, 2018, pp. 158–162.

[17] A. Matsubayashi, Y. Makino, and H. Shinoda, "Direct finger manipulation of 3d object image with ultrasound haptic feedback," in *Proceedings of the 2019 CHI conference on human factors in computing systems*, 2019, pp. 1–11.

[18] A. Matsubayashi, T. Yamaguchi, Y. Makino, and H. Shinoda, "Rendering softness using airborne ultrasound," in *2021 IEEE World Haptics Conference (WHC)*. IEEE, 2021, pp. 355–360.

[19] T. Carter, S. A. Seah, B. Long, B. Drinkwater, and S. Subramanian, "Ultrahaptics: multi-point mid-air haptic feedback for touch surfaces," in *Proceedings of the 26th annual ACM symposium on User interface software and technology*, 2013, pp. 505–514.

[20] T. Iwamoto, M. Tatezono, and H. Shinoda, "Non-contact method for producing tactile sensation using airborne ultrasound," in *Haptics: Perception, Devices and Scenarios: 6th International Conference, EuroHaptics 2008 Madrid, Spain, June 10-13, 2008 Proceedings 6*. Springer, 2008, pp. 504–513.

[21] S. Gupta, D. Morris, S. N. Patel, and D. Tan, "Airwave: Non-contact haptic feedback using air vortex rings," in *Proceedings of the 2013 ACM international joint conference on Pervasive and ubiquitous computing*, 2013, pp. 419–428.

[22] H. Singh, B. Suthar, S. Z. Mehdi, and J.-H. Ryu, "Ferro-fluid based portable fingertip haptic display and its preliminary experimental evaluation," in *2018 IEEE Haptics Symposium (HAPTICS)*. IEEE, 2018, pp. 14–19.

[23] M. R. Longo, "Precise tactile localization on the human fingernail," *Proceedings of the Royal Society B*, vol. 291, no. 2026, p. 20241200, 2024.

[24] I. Birznieks, P. Jenmalm, A. W. Goodwin, and R. S. Johansson, "Encoding of direction of fingertip forces by human tactile afferents," *Journal of Neuroscience*, vol. 21, no. 20, pp. 8222–8237, 2001.

[25] Y. Xu, S. Wang, and S. Hasegawa, "Preserving real-world finger dexterity using a lightweight fingertip haptic device for virtual dexterous manipulation," *arXiv preprint arXiv:2406.16835*, 2024.

[26] A. M. Smith, C. E. Chapman, M. Deslandes, J.-S. Langlais, and M.-P. Thibodeau, "Role of friction and tangential force variation in the subjective scaling of tactile roughness," *Experimental brain research*, vol. 144, pp. 211–223, 2002.

[27] M. Konyo, H. Yamada, S. Okamoto, and S. Tadokoro, "Alternative display of friction represented by tactile stimulation without tangential force," in *Haptics: Perception, Devices and Scenarios: 6th International Conference, EuroHaptics 2008 Madrid, Spain, June 10-13, 2008 Proceedings 6*. Springer, 2008, pp. 619–629.

[28] A. Nahvi, J. Hollerbach, R. Freier, and D. Nelson, "Display of friction in virtual environments based on human finger pad characteristics," in *ASME International Mechanical Engineering Congress and Exposition*, vol. 15861. American Society of Mechanical Engineers, 1998, pp. 179–184.

[29] S. Hasegawa, H. Mitake, and Y. Tazaki, "Springhead: A physics engine for motion and behavior," *Journal of the Robotics Society of Japan*, vol. 30, no. 9, pp. 841–848, 2012.

[30] R. S. Johansson and G. Westling, "Signals in tactile afferents from the fingers eliciting adaptive motor responses during precision grip," *Experimental brain research*, vol. 66, pp. 141–154, 1987.

[31] A. Zangrandi, M. D'Alonzo, C. Cipriani, and G. Di Pino, "Neurophysiology of slip sensation and grip reaction: insights for hand prosthesis control of slippage," *Journal of neurophysiology*, vol. 126, no. 2, pp. 477–492, 2021.

[32] E. M. Young, D. Gueorguiev, K. J. Kuchenbecker, and C. Pacchierotti, "Compensating for fingertip size to render tactile cues more accurately," *IEEE transactions on haptics*, vol. 13, no. 1, pp. 144–151, 2020.

[33] M. Malvezzi, F. Chinello, D. Prattichizzo, and C. Pacchierotti, "Design of personalized wearable haptic interfaces to account for fingertip size and shape," *IEEE Transactions on Haptics*, vol. 14, no. 2, pp. 266–272, 2021.

Yunxiu XU received the B.S. degree from Beijing Information Science and Technology University, Beijing, China, and the M.S. and Ph.D. degrees from the Department of Information and Communications Engineering, Institute of Science Tokyo, Yokohama, Japan, in 2022 and 2025, respectively. He is currently a JSPS Postdoctoral Fellow at The University of Tokyo, Tokyo, Japan, and a Researcher at Institute of Science Tokyo. His research focuses on haptics and interaction in virtual reality.

Siyu Wang received the M.S. degree in Mechanical Engineering from the University of California, San Diego, in 2018. She is currently pursuing the Ph.D. degree with the Department of Information and Communication Engineering, Institute of Science Tokyo, Yokohama, Japan. Her research focuses on soft body simulations using finite element methods and virtual reality.

Shoichi Hasegawa (Member, IEEE) received the D.Eng. degree in computational intelligence and systems from the Tokyo Institute of Technology, Japan. Since 2010, he has been an associate professor with the Institute of Science Tokyo. He was an Associate Professor with the University of Electro Communications, Tokyo. His research interests include haptics, realtime simulations, interactive characters, metaverse, and virtual reality.